ADVANCING EARTH AND SPACE SCIENCE

JGR Solid Earth

RESEARCH ARTICLE
10.1029/2021JB021673

Characteristics of Foreshocks Revealed by an Earthquake Forecasting Method Based on Precursory Swarm Activity

F. Hirose[1], K. Tamaribuchi[1], and K. Maeda[2]

[1]Seismology and Tsunami Research Department, Meteorological Research Institute, Tsukuba, Japan, [2]Seismology and Volcanology Department, Japan Meteorological Agency, Tokyo, Japan

Key Points:

- An earthquake forecast model based on a method that extracts foreshock characteristics is more efficient in forecasting than a stationary epidemic-type aftershock sequence (ETAS) model
- Foreshocks off Iwate prefecture were possibly excited by periodic slow slip events
- In an inland tectonic zone and an island arc, swarm activity associated with magmatic or fluid activity tended to be followed by a mainshock

Supporting Information:

Supporting Information may be found in the online version of this article.

Correspondence to:

F. Hirose,
fhirose@mri-jma.go.jp

Citation:

Hirose, F., Tamaribuchi, K., & Maeda, K. (2021). Characteristics of foreshocks revealed by an earthquake forecasting method based on precursory swarm activity. *Journal of Geophysical Research: Solid Earth*, *126*, e2021JB021673. https://doi.org/10.1029/2021JB021673

Received 7 JAN 2021
Accepted 2 SEP 2021

Abstract We have developed an empirical earthquake forecast method, Maeda's method, based on the statistical features of precursory seismic swarm activity, that is foreshocks, which sometimes appear before a mainshock, and issuing an alert of a mainshock occurrence within a certain period of time. In this study, we investigated the effectiveness of earthquake forecast of Maeda's method by applying it to seismicity under various tectonic environments of Japan such as regions characterized by interplate seismic activity, a tectonic fault line (concentrated deformation zone), and an island arc area of seismic and volcanic activity. As a result, we confirmed that Maeda's method yielded generally higher scores than a forecast model based on a stationary space-time epidemic-type aftershock sequence (ETAS) model. We also found that foreshocks detected along the Japan Trench were distributed along the edges of low-velocity anomalies and among areas with background swarms related to slow slip events (SSEs). The foreshocks may have been caused by a heterogeneous stress distribution associated with the existence of a plate-bending axis and a subducted seamount. Foreshocks off Iwate prefecture, in particular, were excited by periodic SSEs. In an inland tectonic zone and an island arc, swarm activity associated with magmatic or fluid activity related to low-velocity anomalies tended to be followed by a mainshock. Maeda's method is a simple and efficient counting-number-based earthquake forecast model and may capture characteristics of foreshocks that reflect a physical phenomenon, such as a nucleation process involving precursory slip, which the stationary ETAS model is not able to represent.

Plain Language Summary We have developed an empirical earthquake forecast method, Maeda's method, based on the statistical features of precursory seismic swarm activity, that is foreshocks. In this study, we investigated the effectiveness of the earthquake forecast of Maeda's method by applying it to seismicity under various tectonic environments of Japan. As a result, we confirmed that Maeda's method yielded generally higher scores than a forecast model based on a stationary space-time epidemic-type aftershock sequence model. We also found that foreshocks detected along the Japan Trench were distributed along the edges of low-velocity anomalies and among areas with background swarms related to slow slip events (SSEs). In addition, we found that foreshocks off Iwate prefecture in particular were excited by periodic SSEs. In an inland tectonic zone and an island arc, swarm activity associated with magmatic or fluid activity related to low-velocity anomalies tended to be followed by a mainshock. Maeda's method is a simple and efficient counting-number-based earthquake forecast model and may capture characteristics of foreshocks that reflect a physical phenomenon.

1. Introduction

In general, only one particularly large earthquake in a series of seismic activities is called a mainshock, earthquakes that occurred before the mainshock are called foreshocks, and earthquakes that occurred after the mainshock are called aftershocks. If foreshocks can be identified in advance, it will be very useful information for disaster prevention. In the previous study (e.g., Felzer et al., 2004), however, it has been pointed out that there was no correlation between the magnitude of the mainshock and the magnitude, number, and spatial extent of foreshocks, and that aftershocks, multiples, and foreshocks are caused by the same physical process. The aftershock sequence has been simulated well by an epidemic-type aftershock sequence (ETAS) model (Ogata & Katsura, 2014). The ETAS model is represented by the superposition of an epidemic-type aftershock sequence on background activity. Felzer et al. (2015) asserted that an ETAS model with suitable parameters could produce the accelerated increase of the number of earthquakes before mainshocks found by Bouchon et al. (2013). These results indicate that an ETAS model is one of the ef-

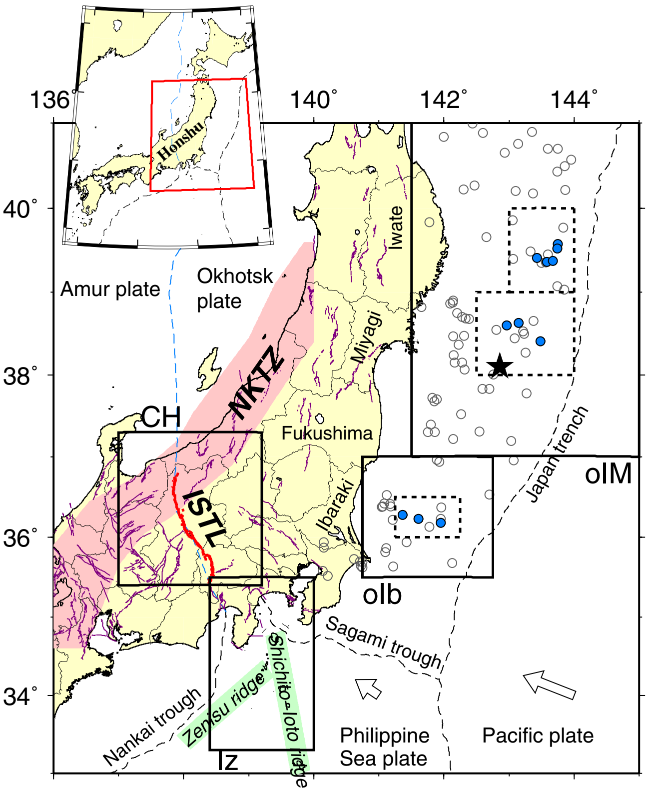

Figure 1. Map of the study regions: oIM, off Iwate and Miyagi prefectures (Figure S1); oIb, off Ibaraki prefecture (Figure S2); CH, central Honshu (Figure S3); Iz, Izu Islands (Figure S5). Circles along the Japan trench indicate the epicenters of target earthquakes preceded (blue solid circles) or not preceded (open circles) by foreshocks, as judged by Maeda's method with $T_f = 9$ days, $N_f = 3$ events, and $T_a = 4$ days (see Section 3.1). In oIM and oIb, areas where target earthquakes tend to be preceded by foreshocks, as defined by Maeda and Hirose (2016), are enclosed by black dashed lines. The star indicates the epicenter of M_w 9.0 Tohoku-oki earthquake, which occurred at 14:46 JST on 11 March 2011 (Hirose et al., 2011). Purple lines indicate active faults, and red lines indicate the Itoigawa-Shizuoka Tectonic Line (Headquarters for Earthquake Research Promotion, 2015a). Thin lines indicate prefectural boundaries. The blue dashed line indicates the boundary at the Earth's surface between the Amur and Okhotsk plates (Bird, 2003). The Niigata-Kobe Tectonic Zone is shown by pink shading (Sagiya et al., 2000). The open arrows indicate the vector of movement of the Pacific and Philippine Sea plates relative to the Okhotsk plate (DeMets et al., 2010). The red rectangle on the inset map indicates the study area.

fective earthquake forecast models because earthquakes are probabilistic phenomena driven by a seismically cascading process.

However, it has been also pointed out that information on foreshock characteristics can provide clues for effective earthquake forecasting because foreshocks are a part of the earthquake nucleation process, which includes precursory slip (Bouchon et al., 2013; Bouchon & Marsan, 2015; Lippiello et al., 2012, 2019). In other words, a simple stationary ETAS model cannot adequately simulate foreshocks (e.g., Seif et al., 2019). Although it is generally quite difficult to distinguish foreshocks from background seismicity before a mainshock occurs, it is known that precursory swarm activity (foreshocks) tends to precede large earthquakes (Maeda, 1993, 1996). Here, the term "swarm" refers to an activity consisting of spatiotemporally close multiple earthquakes except for the mainshock-aftershock type. We previously developed an empirical earthquake forecast method based on the statistical features of precursory swarm activity (Maeda, 1993, 1996; Maeda & Hirose, 2016); we refer to this method as "Maeda's method" hereafter. Maeda's method is a counting-number-based earthquake forecast model in which if several earthquakes excluding small aftershocks have occurred in a certain area within a few days, an alert that a mainshock will occur in the same area within the next few days is issued. Previous studies (Maeda, 1993, 1996; Maeda & Hirose, 2016) mainly described the forecast performance by Maeda's method, and the physical interpretation for foreshocks was poor. In recent years, various findings have been obtained from dense microseismic monitoring (Mochizuki et al., 2008; Nishikawa et al., 2019; Uchida et al., 2016), seismic tomography (Hua et al., 2020; Nakajima & Hasegawa, 2007), and airgun survey (Fujie et al., 2006; Kodaira et al., 2007; Tsuru et al., 2002) under various tectonic environments. Therefore, we attempted to physically interpret foreshocks through these new findings.

We focused our investigation on four specific regions of Japan: off Iwate and Miyagi prefectures, off Ibaraki prefecture, central Honshu (the main island of Japan), and the Izu Islands, where foreshock activity is particularly common (Maeda, 1993, 1996; Maeda & Hirose, 2016) (Figure 1). The first two of these regions are characterized by interplate seismic activity, the third includes a tectonic fault line (concentrated deformation zone), and the fourth is an island arc area of seismic and volcanic activity. For each region among various tectonic environments, we showed the effectiveness of earthquake forecast by Maeda's method and discussed the physical characteristics of the extracted precursory swarm activity. To investigate whether Maeda's method merely captures apparent foreshocks due to the aftershock trigger effect expressed by the ETAS model, we also compared the results with an earthquake forecast model based on the stationary space-time ETAS model and applied Maeda's method to synthetic ETAS catalogs.

2. Data and Study Regions

We used the Japan Meteorological Agency (JMA) unified hypocenter catalog (JMA catalog hereafter). JMA classifies and flags data according to their accuracy and determination method (https://www.data.jma.go.jp/svd/eqev/data/bulletin/catalog/notes_e.html). For high-precision hypocenters (flags K, k, and A) in our study regions, the origin time error is less than 0.5–1.0 s and the epicenter latitude/longitude estimation error is less than 3.0–5.0 min. For low-precision hypocenters (flags S, s, and a), typically in areas with a low density of stations such as around minor islands, the origin time error is less than 0.5–2.0 s and the epicenter

Table 1
Data Selection Criteria

	Period		Region				# Of earthquakes		
Area	Years	Days	Latitude (°N)	Longitude (°E)	Depth (km)	M_{th}	Total	K, k, A	S, s, a
Off Iwate	1961–2010	18,262	39.0–40.0	143.0–144.0	0.0–100.0	5.0	250	247	3
Off Miyagi	″	″	38.0–39.0	142.5–144.0	″	″	90	90	0
Off Ibaraki	″	″	36.0–36.5	141.25–142.25	″	″	102	102	0
Central Honshu	1998–2019	8035	35.6–37.1	137.2–139.0	0.0–30.0	2.0	5805	5799	6
Izu Islands	1977–2019	15,705	33.5–35.3	138.6–139.8	0.0–50.0	3.0	8488	8293	195

Note. K, k, A = high-precision hypocenters; S, s, a = low-precision hypocenters.

latitude/longitude estimation error is less than 3.0–10.0 min. In this study, we used all classes of data because the information about whether or not an earthquake occurred was useful even if the location error was not small. However, low-frequency earthquakes were excluded. Previous studies (Maeda, 1993, 1996; Maeda & Hirose, 2016) used only hypocenters flagged K. Flags k, A, s, and a were first introduced in April 2016 (Tamaribuchi, 2018). In general, fewer earthquakes have flags S, s, and a, compared with the number with flags K, k, and A (Table 1). Information on seismicity in each of our study regions is given in the Supporting Information S1, Section S1.

3. Methods

3.1. Maeda's Method: An Empirical Earthquake Forecast Method

Maeda's method (Maeda, 1993, 1996; Maeda & Hirose, 2016) is a forecast model that efficiently extracts foreshocks from background seismicity.

3.1.1. Foreshock Identification Procedure

The method used to search for parameters of foreshocks that show high forecast performance consists of the following four steps:

1. Elimination of small aftershocks from the original data. Distance L (km) and the time interval t_a (days) between a mainshock and an aftershock depend on the magnitude of a previous earthquake (M_{pre}) as

$$\log_{10} L \leq 0.5M_{pre} - 1.8, \tag{1}$$

$$\log_{10}\left(t_a + 0.3\right) \leq \left\{0.17 + 0.85\left(M_{pre} - 4.0\right)\right\}/1.3, \tag{2}$$

where Equations 1 and 2 are basing on empirical laws proposed by Utsu (1961) and Utsu (1970), respectively, to identify aftershocks. For example, when M_{pre} is 8, 7, and 6, L is 160, 50, and 16 km, respectively, and t_a is 557, 123, and 27 days, respectively. To remove only small earthquakes, we introduced the following condition:

$$M_a < M_{pre} - M_d; \quad M_d = 1.0, \tag{3}$$

where M_a is the magnitude of an aftershock, and M_d represents the magnitude difference between M_{pre} and M_a. The reason for including Equation 3 is that earthquake swarm activity with small magnitude differences may be connected to a subsequent larger event. Note that although it has been reported that small aftershock data are missing in catalogs due to overlapping seismic waveform records for about one day immediately after a large earthquake (Zhuang et al., 2017), Maeda's method can avoid the problem of short-term aftershock incompleteness by not dealing with small earthquakes.

2. Selection of foreshock (precursory swarm activity) candidates, defined as the number N_f of earthquakes with magnitude $\geq M_{f0}$ (the foreshock magnitude threshold) occurring in a segment with size $D° \times D°$ (latitude × longitude) during a period of T_f days. Grid points at the centers of segments in the evaluation area are spaced at intervals of $D°/2$ (red crosses in Figures S1a and S5a). The alarm area is the same

Table 2
Optimum Parameters and Results Obtained by Applying Maeda's Method to the Real Catalog

		Parameter						Alarm rate		Truth rate				
Area	Period	D (°)	M_{f0}	T_f (days)	N_f	T_a (days)	M_{m0}	(%)		(%)		F (%)	PG	ΔAIC
Off Iwate and Miyagi	1961–2010	0.5	5.0	9	3	4	6.0	33.3	(= 8/24)	24.4	(= 10/41)	28.2	340.5	78.3
Off Ibaraki	"	"	"	3	2	1	"	66.7	(= 4/6)	30.8	(= 4/13)	42.1	1567.5	52.5
Central Honshu	1998–2019	0.2	2.0	1	5	5	5.0	40.0	(= 6/15)	9.6	(= 7/73)	15.5	439.9	61.9
Izu Islands	1977–2019	0.2	3.0	1	2	4	5.0	72.3	(= 47/65)	20.1	(= 63/314)	31.4	338.0	499.2

segment with size $D° \times D°$. The N_f-th foreshock candidate in each sequence is called an alarm earthquake in this paper

3. Selection of the alarm period. The alarm period T_a is the number of days after an alarming earthquake is used to forecast a target earthquake
4. The values of D, M_{f0}, T_f, N_f, T_a, and M_{m0} (the mainshock magnitude threshold) that result in a high forecast performance are determined by the grid-search method. See Section 3.1.2 for forecast efficiency

Earthquakes with $M \geq M_{m0}$, excluding aftershocks (earthquakes that satisfy Equations 1 and 2), are defined as target earthquakes. We applied Maeda's method to the real catalog to obtain the optimum values of parameters D, M_{f0}, T_f, N_f, T_a, and M_{m0} in each study region. In this regard, for optimum values of M_{f0} and M_{m0}, and for optimum values of D in the areas along the Japan trench, we used the values determined by Maeda and Hirose (2016) in order to save calculation cost. To determine optimum values for D in central Honshu and the Izu Islands, we tested three possible values (Table S1). We estimated values for the other parameters by the grid search method from 900 combinations because it is sensitive to earthquake catalog: $T_f = 1, 2, ..., 10$ days; $N_f = 2, 3, ..., 10$ events; and $T_a = 1, 2, ..., 10$ days. The optimum parameter values and forecast results (see Section 3.1.2) in each region in this study (Table 2) are different from those in the previous studies (Maeda, 1993, 1996; Maeda & Hirose, 2016) because of differences in the data precision flags, evaluation regions (this study considered only specific areas along the Japan trench), and analysis periods.

3.1.2. Indices of Forecast Efficiency

We adopted the difference in the Akaike information criterion, ΔAIC (the same as PIC of Maeda, 1996), an information theory-based criterion, as an index of the overall performance of a forecast algorithm:

$$\Delta\mathrm{AIC} = 2nAR\ln\mathrm{PG} + 2n\left(1-\mathrm{AR}\right)\ln\frac{1-\mathrm{AR}}{1-\dfrac{\mathrm{AR}}{\mathrm{PG}}} - 2 \quad \left(\mathrm{PG} \geq 1\right), \tag{4}$$

where n represents the total number of target earthquakes, AR is the alarm rate (= [number of target earthquakes in alarmed space-time]/[total number of target earthquakes]), and PG is the probability gain (= [occurrence rate of target earthquakes in alarmed space-time]/[background occurrence rate]). Equation 4 calculates ΔAIC between two models: a uniform Poisson model and a two Poisson rate model. The latter assumes that the Poisson rate in the alarmed space-time is different from the rate in non-alarmed space-time. A ΔAIC value of less than about two is considered insignificant (Utsu, 1999). PG can also be used to evaluate the performance of a forecast model; when PG < 1, the forecast model is inferior to the uniform Poisson model. Note that PG becomes large if the background region includes an area where no earthquakes are expected to occur. To avoid that problem, we excluded segments ($D° \times D°$) where no earthquakes with magnitude $\geq M_{f0}$ occurred during the entire period used to calculate PG. The truth rate (TR) (= [number of alarm earthquakes followed by a target earthquake in alarmed space-time]/[total number of alarm earthquakes]), is another index of forecast efficiency. There is a trade-off between AR and TR (or PG). Therefore, we used ΔAIC to evaluate forecast efficiency comprehensively and also used the F-measure, defined as the harmonic mean of AR and TR, as a supplemental index of forecast efficiency. For each of these five indices of forecast efficiency, the larger the index value, the better the forecast performance. Note that because ΔAIC depends on the number of target earthquakes, ΔAIC should not be compared between different target earthquakes.

3.2. Forecast Model Based on the Stationary Space-Time ETAS Model

Equation 4 shows the difference in forecast performance between Maeda's method and random guess. We would like to also compare with a more advanced forecast model than random guess and evaluate quantitatively whether Maeda's method merely captures apparent foreshocks due to the aftershock trigger effect. Therefore, we adopted a forecast model based on the stationary space-time ETAS model (Ogata & Zhuang, 2006) (hereinafter, ETAS forecast model) as a reference. It has been pointed out that the stationary ETAS model whose parameters do not change with time does not reproduce foreshocks well (Seif et al., 2019). In addition, the nonstationary ETAS model with time-dependency in the background seismicity rate (Llenos et al., 2009; Kumazawa & Ogata & Katsura, 2014), the ETAFS model that foreshocks with reverse time have similar characteristics to spatiotemporal decay of aftershocks (Petrillo & Lippiello, 2021), and an ensemble forecast consisting of various ETAS models with different parameters (Llenos & Michael, 2019) have also been proposed. Our study area is the area where the forecast performance of Maeda's method for detecting precursory swarm activity is relatively high (Maeda, 1993, 1996; Maeda & Hirose, 2016), so it may be at a disadvantage for the stationary space-time ETAS model which is pointed out to be low reproducibility of foreshocks. However, because the purpose of this study is not to improve the forecast efficiency of the ETAS forecast model, we adopted the standard stationary space-time ETAS model here (see Section S2). Note that because the ETAFS model (Petrillo & Lippiello, 2021) is a model that uses information on future events, it cannot be used in principle for forecast. See Section S2 for details of the construction procedure and evaluation of the ETAS forecast model.

Besides that, for off Iwate and Miyagi prefectures and off Ibaraki prefecture along the Japan Trench, we constructed synthetic catalogs based on the stationary space-time ETAS model (ETAS catalogs, hereafter). By applying Maeda's method to the ETAS catalogs, we also investigated whether Maeda's method merely captures apparent foreshocks due to the aftershock trigger effect expressed by the ETAS model (Section S3). See Section S4 for details of the construction procedure of ETAS catalogs.

4. Forecast Performance

4.1. Comparison of Forecast Results Between Maeda's Method and ETAS Forecast Model

Figure 2 summarizes forecast results of Maeda's method (Table 2) and ETAS forecast model (Table S3). For the ETAS forecast model, results with the highest ΔAIC in each region are plotted. In a few cases, the results of the ETAS forecast model are better than Maeda's one depending on indices of forecast efficiency (Section 3.1.2) such as AR and PG (Figures 2a and 2d). However, because ΔAIC and the F-measure of Maeda's method is higher than that of the ETAS forecast model (compared with the same color in Figure 2), Maeda's method has higher forecast performance comprehensively. In the example of applying the ETAS forecast model to seismicity in and around Italy, PGs exceeded 100, but TRs were a few percent, indicating that practical application would be difficult (Console et al., 2010). The same tendency for the ETAS forecast model can be seen in Figure 2. In this study, PGs of both forecast models in Figure 2d are larger than those of other forecast models (see Nakatani, 2020, for a review of the PGs of various forecast models). Especially, the forecast efficiency with Maeda's method tends to be large because the alarmed time-space is very small, resulting in that PGs, AR, and TR reached about 300%–1600%, 30%–70%, and 10%–30% (Figure 2, Table 2). Even though Maeda's method is a simple counting-number-based earthquake forecast model, it produces a comprehensively more efficient forecast than a complex ETAS forecast model.

4.2. Temporal Acceleration of Foreshocks Before Target Earthquakes

Figure 3 shows the cumulative number of stacked earthquakes, normalized by the number of target earthquakes and the maximum number of foreshocks just before the mainshock and excluding earthquakes satisfying the aftershock conditions (Equations 1–3 in Section 3.1.1), in the 30 days before the target earthquakes in each target area (Figure 3). The spatial range of each target earthquake is $D° \times D°$ centered on the grids (red crosses in Figures S1a and S5a).

The temporal acceleration of the cumulative number of foreshocks prior to a target earthquake is apparent in all regions. Figures 3c and 3d show the dependency of magnitudes of target earthquakes in central

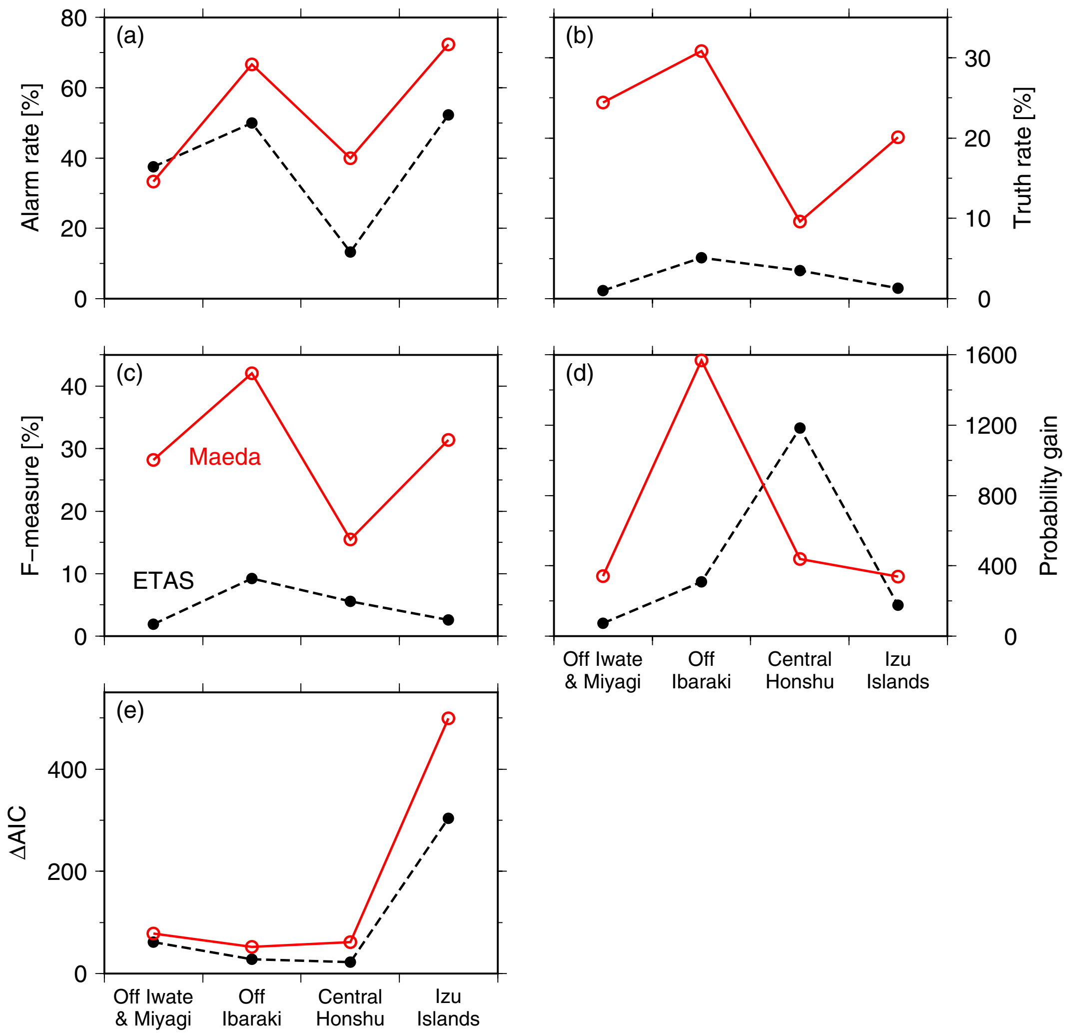

Figure 2. Forecast results. (a) Alarm rate, (b) truth rate, (c) F-measure, (d) probability gain, and (e) Akaike Information Centre (ΔAIC). Red and black symbols indicate forecast results by Maeda's method and the ETAS forecast model with the highest ΔAIC (Table S3), respectively.

Honshu and the Izu Islands, respectively. We can find the temporal acceleration at any target magnitudes, and the larger the target magnitude is, the more remarkable the temporal acceleration is.

For two regions (off Iwate and Miyagi prefectures and off Ibaraki prefecture) along the Japan Trench, we also superimpose the average of 1,000 synthetic ETAS catalogs in Figures 3a and 3b (see Section S3). We can find the temporal acceleration in both the real catalog (red curve) and the average of the ETAS catalogs (blue curve). Results obtained by applying Maeda's method with the optimum parameter values for each ETAS catalog to 1,000 synthetic ETAS catalogs are shown in Table S5, Figures S12h–S12k and S13h–S13k. The median PG is several hundred. Because Maeda's method has the property of extracting foreshocks, these results indicate that foreshocks could be reproduced to some extent just by superimposing aftershock triggering effects and random background activity, as pointed out in previous studies (e.g., Felzer et al., 2015). However, on the other hand, the seismicity immediately before target earthquakes was more active in the real catalog (Figure 3), and the comprehensive forecast efficiency index F-measure was higher when Maeda's method is applied to the real catalog (Table 2). These results indicate that it is hard for the stationary space-time ETAS model to reproduce foreshock characteristics well, as pointed out in previous studies (e.g., Seif et al., 2019). Note that Maeda's method adopted parameters that maximize ΔAIC as optimum parameters, but as described in Section 3.1.2, ΔAIC depends on the number of target earthquakes. Because the

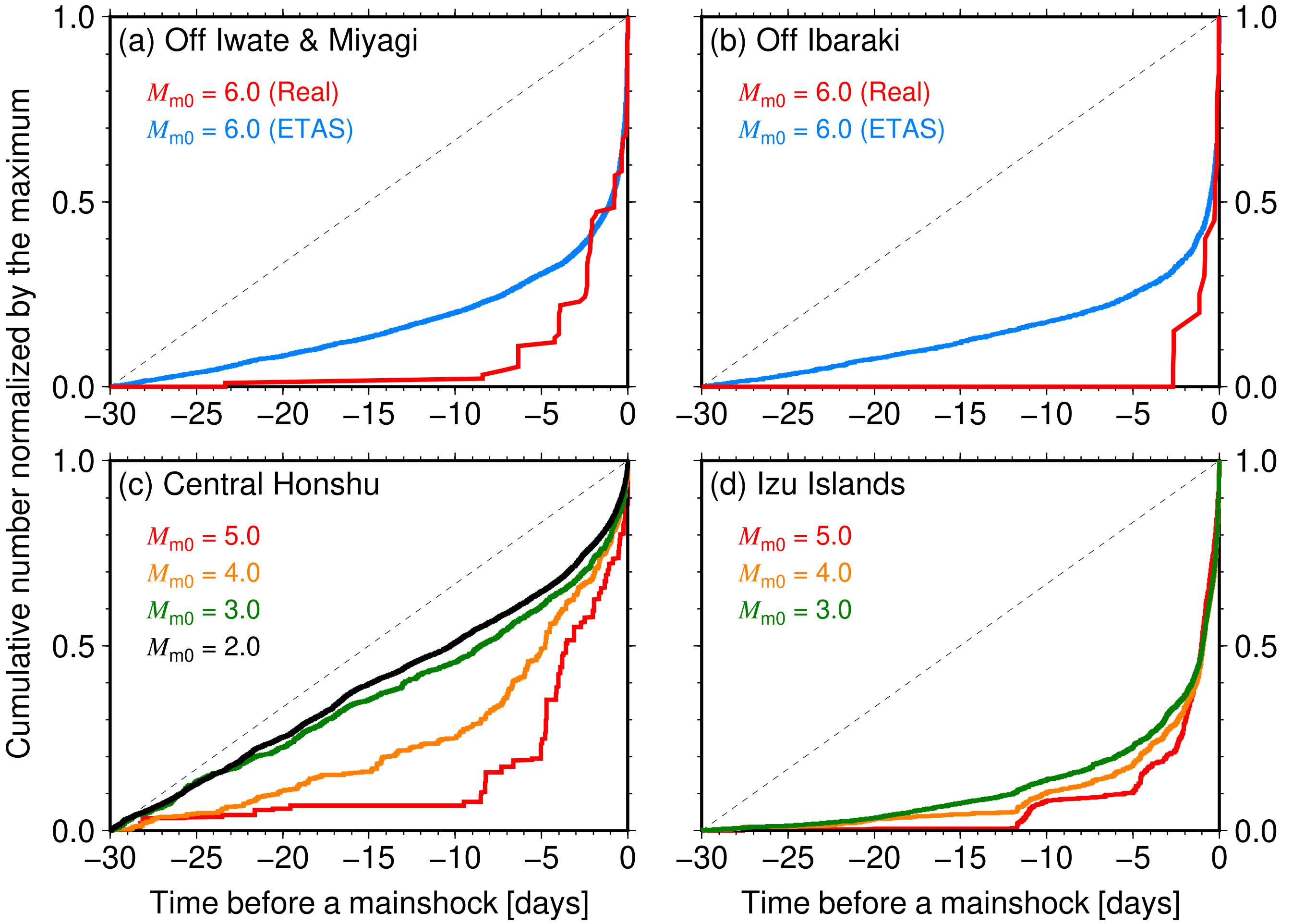

Figure 3. Cumulative number of stacked earthquakes in the 30 days before a mainshock (target earthquake). The cumulative number is normalized by the number of mainshocks and the maximum just before mainshocks. Earthquakes satisfying the aftershock conditions (Equation 1–3) have been excluded. (a) Off Iwate and Miyagi prefectures, (b) off Ibaraki prefecture, (c) central Honshu, and (d) Izu islands. A blue curve in (a), (b) indicates the average of each track of 1,000 synthetic catalogs (see Figure S11). Other curves indicate a track depending on a magnitude threshold of target earthquakes of the Japan Meteorological Agency catalog.

ETAS catalog and the real catalog have different target earthquake numbers (Figures S12b and S13b), the comparison of ΔAICs is not shown in Table S5, Figures S12h–S12k and S13h–S13k.

To summarize, Maeda's method is a simple and efficient counting-number-based earthquake forecast model and may capture characteristics of foreshocks that reflect a physical phenomenon, such as a nucleation process involving precursory slip, which the stationary ETAS model is not able to represent.

5. Spatio-Temporal Characteristics of Regions Where Foreshocks Tend to Occur

In this section, we describe the spatiotemporal characteristics of target earthquakes and alarm earthquakes based on the results (Table 2) obtained by applying Maeda's method to real data.

5.1. Spatial Features Along the Japan Trench

As shown previously (Maeda, 1996; Maeda & Hirose, 2016), target earthquakes are preceded by foreshocks (blue circles in Figure 4) and alarm earthquakes followed by a target earthquake (red circles in Figure 4) tend to be distributed in specific areas along the Japan trench. In the results obtained by applying optimum

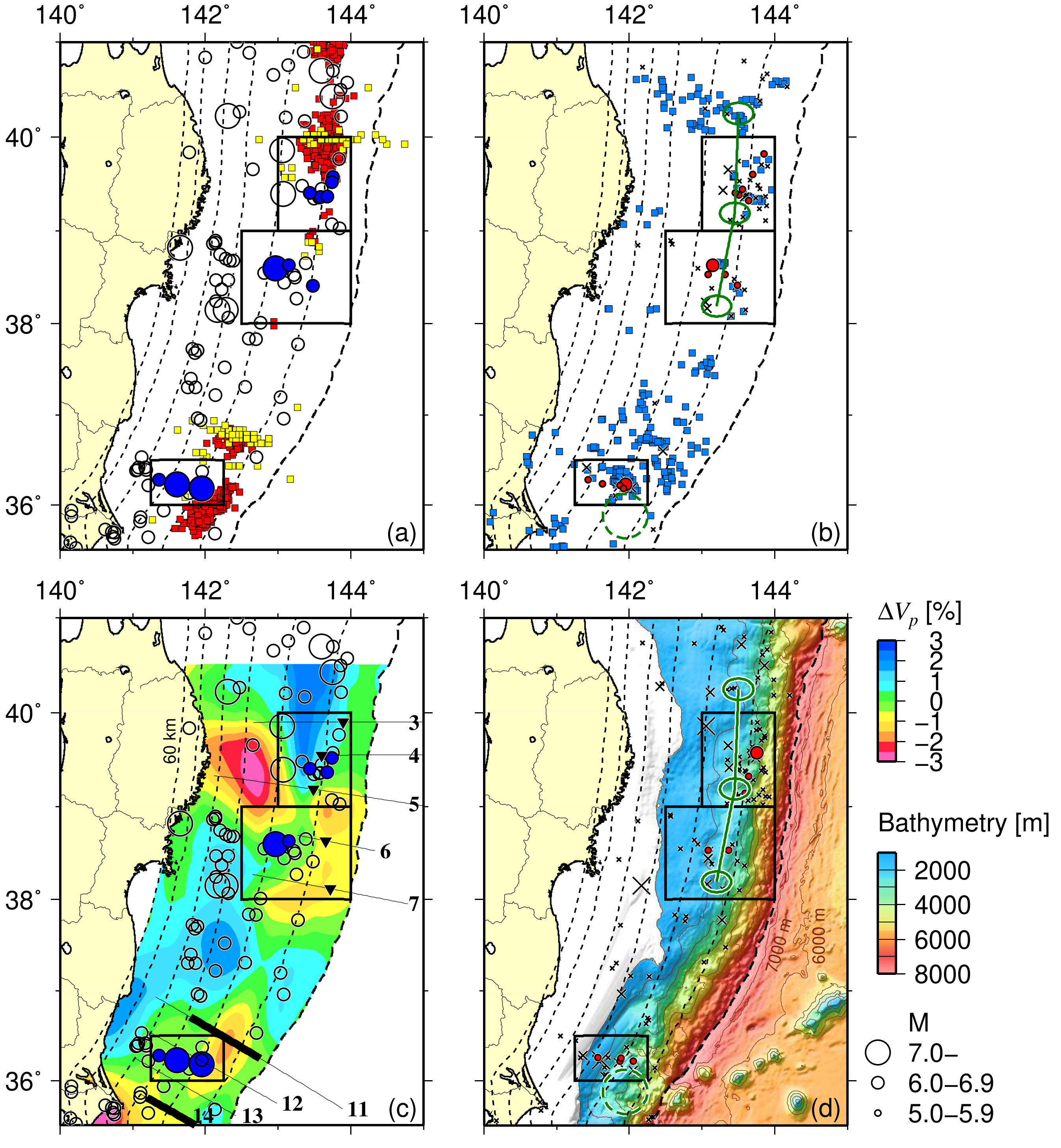

Figure 4.

parameters (Table 2) for off Iwate and Miyagi prefectures and off Ibaraki prefecture, respectively, to all earthquakes along the Japan trench (upper and lower panels in Figure 4), alarmed target earthquakes and true alarm earthquakes were concentrated in specific areas even when the foreshock parameters differed. In margins (latitudes 40°, 39°, 38°, 36.8°, and 36°N) of these specific areas, tremors and very low frequency earthquakes also occurred (Nishikawa et al., 2019) (Figure 4a), but regular seismicity was low (Figures S1 and S2), indicating a low interplate coupling rate. Background swarms identified by deviations from an

ETAS model are considered to correspond to slow slip events (SSEs) (Nishikawa et al., 2019). The background swarm distribution complements the distributions of tremors and very low frequency earthquakes, except off the boundary between Fukushima and Ibaraki prefectures (cf. Figures 4a and 4b). Most alarm earthquakes, however, are distributed in the background swarm areas (Figure 4b), indicating that swarm-like activity (alarm earthquakes), which is sometimes linked to large earthquakes (target earthquakes), is possibly related to SSEs. However, this result also suggests that the properties of background swarms differ among areas because true alarm earthquakes have more limited distribution.

Maeda (1996) reported regional variations of foreshocks along and across the trench and suggested that these variations may be caused by stress concentration driven by high structural heterogeneity at the plate boundary due to, for example, subducting seamounts, variations in the thermal structure, and subduction zone rheology.

Hua et al. (2020) estimated seismic velocity perturbations along the upper boundary of the subducting Pacific slab (Figure 4c) using high-quality data recorded by dense seismograph networks on land and seafloor. They showed that the 2011 Tohoku-oki earthquake (M_w 9) initiated at a boundary between a down-dip high-velocity anomaly and an up-dip low-velocity anomaly. They suggested that the low-velocity anomaly at shallow depth indicates low-rigidity materials, such as subducted sediments, and an increase of dynamic pore-fluid pressure. They interpreted that the weak materials could not arrest the strong inertial motion of rupture propagating from down-dip, resulting in the large slips near the trench. In addition, they pointed out that the strong high-frequency radiation and strong ground motions mainly originated in the high-velocity anomaly in the deeper portion. Epicenters with $M \geq 7$ during 1917–2011 were distributed outside of the low-velocity anomaly areas. The distribution of background swarms (Figure 4b), extracted by Nishikawa et al. (2019), does not correspond spatially to the seismic velocity structure (Figure 4c). In contrast, alarmed target earthquakes and true alarm earthquakes identified by Maeda's method are distributed along the edges of the low-velocity anomaly areas.

Tsuru et al. (2002) conducted multichannel seismic reflection surveys and identified a wedge-shaped low-velocity zone at the tip of the overriding continental plate in the northern area of the Japan trench. They suggested that wedge-shaped low-velocity units may be caused by the presence of fluid and contribute to reduced coupling at the plate boundary. The distributions of alarmed target earthquakes and true alarm earthquakes do not correspond spatially to the wedge-shaped low-velocity units (Figure 4c); therefore, their presence does not constrain the occurrence of foreshocks. This interpretation is also supported by the lack of a wedge-shaped low-velocity unit in the area of foreshock activity off Ibaraki prefecture. However, Tsuru et al. (2002) identified a channel-like low-velocity layer with a thickness of a few kilometers (thick lines 11 and 14 in Figure 4c) off Ibaraki prefecture. They suggested that the presence of fluid can also cause a subduction channel and contribute to reduced coupling at the plate boundary. In fact, seismicity is low in those areas (Figure s2) where tremors and very low frequency earthquakes are also observed (Nishikawa et al., 2019) (Figure 4a). Subduction channels may be formed by the subduction of multiple seamounts, where strain energy is lost because of erosion of the base of the overriding plate (Mochizuki et al., 2008).

Mochizuki et al. (2008) investigated the relationship between seismicity and a large subducted seamount on the basis of ocean-bottom seismometer observations. They inferred that a subducted seamount may have concentrated stress at its northern subduction front, where they observed seismicity during about one month of observation and where the July 1982 M 7 earthquake rupture started. They also reported that aftershocks of repeated large earthquakes of $M \sim 7$ with a recurrence interval ∼20 years since the 1920s did

Figure 4. Forecast results along the Japan trench obtained by applying Maeda's method to the Japan Meteorological Agency catalog with (a), (b) $T_f = 9$ days, $N_f = 3$ events, and $T_a = 4$ days or (c), (d) $T_f = 3$ days, $N_f = 2$ events, and $T_a = 1$ day (a), (c) Epicentral distributions of target earthquakes preceded by (solid blue circles) or not preceded by (open circles) foreshocks. (b), (d) Epicentral distributions of foreshock candidates (alarm earthquakes) followed by (solid red circles) or not followed by (x marks) a target earthquake. In addition to the forecast results, the following information is superimposed: (a) Tremors with a duration of 80 s or longer (red squares) and very low frequency earthquakes (yellow squares) (Nishikawa et al., 2019). (b) Background seismicity swarms (blue squares) (Nishikawa et al., 2019). (c) Residual P-wave velocity perturbations along the upper boundary of the subducting Pacific slab (Hua et al., 2020). Red and blue tiles indicate low-and high-velocity anomalies, respectively. The dashed lines are depth contours of the upper boundary of the subducting Pacific slab (contour interval 10 km) (Hua et al., 2020). Thin lines indicate seismic reflection survey lines. The inverted triangles on lines 3–7 indicate the western edge of a wedge-shaped unit with a P-wave velocity of 2–3 km/s. The thick parts of lines 11 and 14 indicate the location of a channel-like unit with a P-wave velocity of 3–4 km/s (Tsuru et al., 2002). (d) Bathymetry (contour interval 1,000 m). In (b), (d), the green ellipses indicate plate-bending points, and the line connecting the bending points indicates the bending axis (Fujie et al., 2006), and the green dashed circle indicates the subducted seamount (Mochizuki et al., 2008).

not occur south of the subducted seamount, indicating that the subducted seamount itself may not define the rupture area or cause low coupling. True alarm earthquakes also tended to be distributed along the northern edge of a subducted seamount (Figure 4d). Accordingly, foreshock occurrence may be affected by stress heterogeneities and stress concentrations associated with the existence of subducted seamounts.

Fujie et al. (2006) defined a plate-bending axis by connecting three bending points, where the dip of the subducting plate changes markedly, off Iwate and Miyagi prefectures (green line in Figures 4b and 4d). They pointed out that the bending axis approximately coincides with the updip limit of the rupture zone of large (M 7–8) interplate earthquakes, and velocities at the bottom of the upper plate vary from east to west across the bending axis. Thus, they interpreted that a change of physical properties in the upper plate may affect the configuration of the subducting plate and stress accumulation. They also observed microseismic activity along the bending axis. In our results, true alarm earthquakes appear to be distributed around the plate-bending axis. If the large subducted seamount off Ibaraki prefecture is also considered to be a plate-bending point, it is interesting to note that the depth of that bending point is the same as that of the bending points off Iwate and Miyagi prefectures.

To summarize, the distribution of true foreshocks that preceded large earthquakes (target earthquakes) is limited to the edges of low-velocity anomalies in areas of background seismicity swarms that are related to SSEs. Also, those foreshocks may be caused by a heterogeneous stress distribution associated with the existence of a plate-bending axis and a large subducted seamount.

5.2. Relation With SSEs

Off Iwate and Miyagi prefectures, 8 of 24 target earthquakes were alarmed (AR 33.3%; Table 2 and Figure 5), and 10 of 41 alarm earthquakes were true foreshocks (TR 24.4%). The number of alarmed target earthquakes is not always the same as the number of true alarm earthquakes because an alarm may be associated with multiple target earthquakes.

Uchida et al. (2016) identified periodic SSEs with recurrence intervals of 1–6 years on interplate areas along the Kuril and Japan trenches by analyzing repeating earthquakes catalog and GNSS data. Offshore Sanriku (pink dashed rectangle in Figures 5a and 5b), the dominant slip period of SSEs was 3.09 years. In region N (Figure 5), all 14 target earthquakes synchronized with the positive phase of the best-fitted sinusoidal function to the 3.09-year SSE period (pink and gray stripes in Figures 5c and 5d). Binomial testing indicated that the probability of this occurring by chance was 0.006%. Similarly, 19 of 27 alarm earthquakes (∼70%) synchronized with the SSE period (Figure 5d), and a binomial test showed the probability of this being by chance was 2.6%. Moreover, all alarmed target earthquakes and alarm earthquakes synchronized with the SSE periods. We also evaluated the correlation between foreshocks and SSEs using Molchan's error diagram (Molchan, 1997). As a result, Molchan's error diagram also showed that both target and alarm earthquakes significantly synchronized with the positive phase of the sinusoidal curve with the 3.09-year period off Iwate prefecture (Figure S14), although alarm earthquakes are less significant than target ones. SSEs might facilitate cascading ruptures (Noda et al., 2013) and thus lead to a large-magnitude rupture (target earthquake). Accordingly, foreshocks detected by Maeda's method may be excited by SSEs.

However, one example shows that seismicity swarms do not always lead to a target earthquake. In region N, alarm earthquakes occurred occasionally during 1974–1988 without being followed by a target earthquake (Figures 5c and 5d). Noda et al. (2013) showed by a rate and state simulation of faults with a hierarchical asperity model, in which a large, tough patch includes smaller fragile patches, that only small patches ruptured without a cascade-up process occurring because of the high strength of the large patch. During 1974–1988, the plate boundary status might have been characterized by a high coupling rate. Although the catalog of small repeating earthquakes does not cover the entire 1974–1988 period, the slope of the averaged cumulative slip of repeating earthquakes during 1984.5–1988 in region N (green curves in Figures 5c and 5d) is gentler than the slope in later periods, indicating a higher interplate coupling rate. In addition, the fact that only three of the nine alarm earthquakes (∼33%) synchronized with the SSE periods during 1974–1988 suggests that the interplate coupling status differed during that period compared with the status both before 1974 and after 1988.

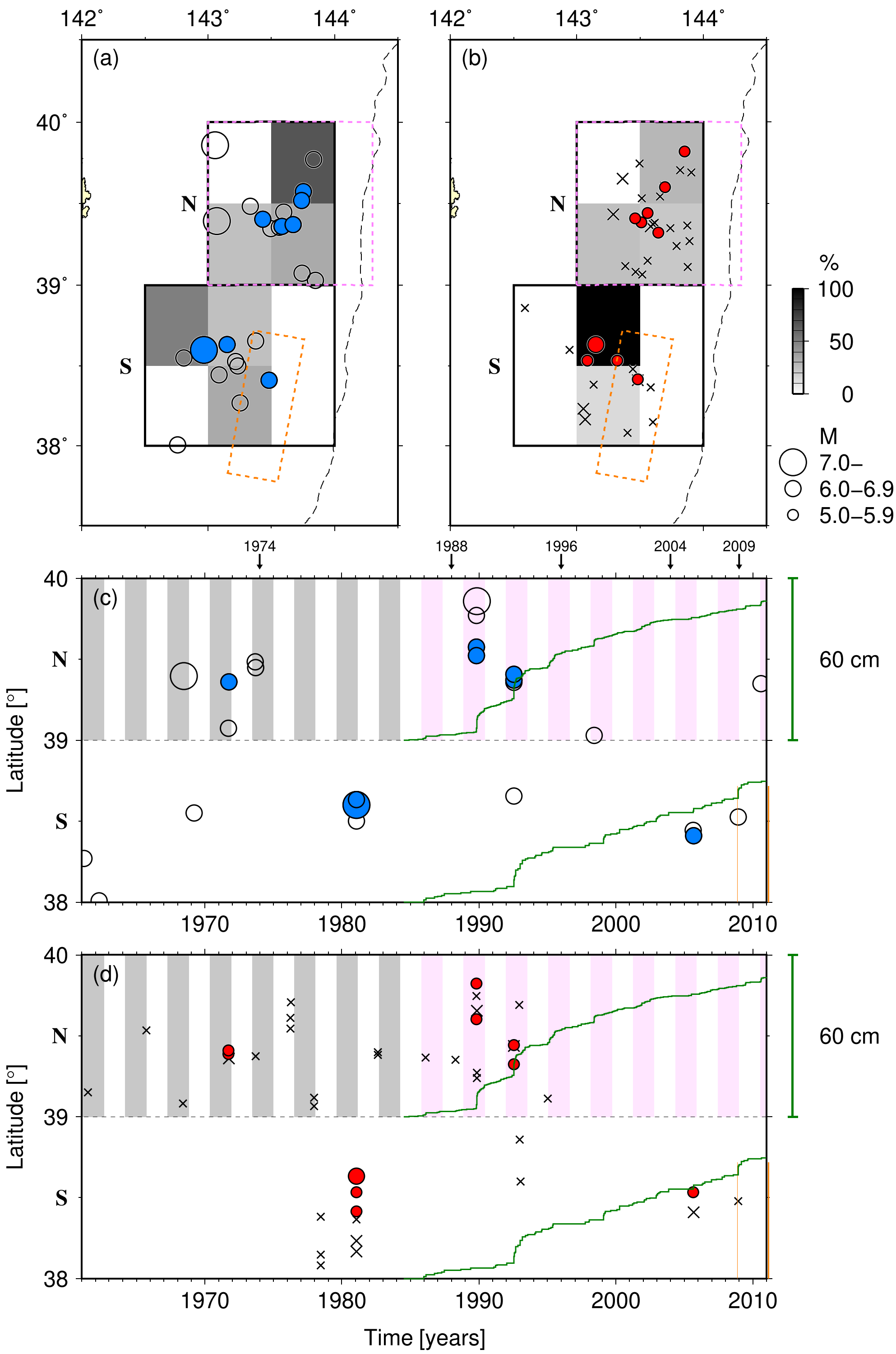

Figure 5.

The number of not only target earthquakes but also alarm earthquakes decreased after 1996. The slope of the averaged cumulative slip of repeating earthquakes after 1996 in region N is gentler than that during 1989–1995 and steeper than that during 1984.5–1988, indicating moderate interplate coupling. During 2004–2009, the slope is the same as during 1984.5–1988, and the periodicity of SSEs also collapsed (see

Figure 2b of Uchida et al., 2016). Therefore, the interplate coupling status may have been similar during 1984.5–1988 and 2004–2009.

In region S, the repeating earthquakes analysis showed no SSE periodicity (see Figure 4 of Uchida et al., 2016). Using ocean-bottom pressure data, Ito et al. (2013) estimated that an SSE of M_w 6.8 occurred in November 2008 and one of M_w 7.0 occurred in February 2011 in a part of region S. A target earthquake and an alarm earthquake occurred almost in synchronization with the 2008 SSE shown by orange lines in Figures 5c and 5d. Accordingly, foreshocks also in region S might be excited by SSEs.

Off Ibaraki prefecture, four of six target earthquakes were alarmed (AR 66.7%; Table 2, Figure 6), and 4 of 13 alarm earthquakes were true foreshocks (TR 30.8%). In area H off Ibaraki prefecture (pink dashed rectangle in Figures 6a and 6b), the excitation period of SSEs was 2.53 years (Uchida et al., 2016). Four of six target earthquakes and 6 of 13 alarm earthquakes synchronized with the SSE period (pink and gray stripes in Figures 6c and 6d). The one-sided testing probabilities of chance occurrence were 34.3% and 70.9%, respectively, by the binomial test, so the null hypothesis could not be rejected with a significance level of 5%. During 1997–2005, however, the periodicity of SSEs was not clear in area H (Figure S3 of Uchida et al., 2016). Furthermore, the averaged cumulative slips of repeating earthquakes in the evaluation area did not show a clear periodicity of SSEs in this study (green curve in Figures 6c and 6d). Therefore, these target and alarm earthquakes seem to lack periodicity. However, because background swarm activity related to SSEs (Nishikawa et al., 2019) occurs off Ibaraki prefecture (Figure 4b), the foreshocks may be related to non-periodic SSEs.

To summarize, foreshocks extracted from swarm activity by Maeda's method may be excited by SSEs, and foreshocks off Iwate prefecture, in particular, are excited by periodic SSEs.

5.3. Central Honshu

In central Honshu, we adopted $D = 0.2°$ because it yielded the maximum ΔAIC among the three tested values (Table S2). Six of 15 target earthquakes were alarmed (AR 40.0%; Figure 7) of 73 alarm earthquakes were true foreshocks (TR 9.6%). Two events among the six alarmed target earthquakes occurred along the ISTL, and five occurred in the NKTZ (Figure 1). The AR was relatively high in the grids in these areas.

Many earthquakes were induced throughout Japan by the M_w 9.0 Tohoku-oki earthquake, which occurred at 14:46 JST on 11 March 2011 (Hirose et al., 2011). Alarm earthquakes also increased just after the M_w 9 event (Figure 7d). One induced earthquake was event C (M 6.7), which occurred about 13 h after the Tohoku-oki earthquake (Figure 7c). Maeda's method automatically judged event C to be an alarmed target earthquake. However, only one foreshock candidate had occurred in the aftershock area of event C (crosses in Figure S4); in addition, $N_f = 5$, indicating that event C had little relation to the alarm earthquake and swarm activity around 36.8°N. Because this isolated swarm activity occurred over a short time interval, Maeda's method may have incorrectly judged it to be a true foreshock. Accordingly, event C has characteristics different from those of other alarmed target earthquakes. If we take this into account, we can see that the features of foreshocks in the NKTZ differ to the east and west of Mt. Niigata-Yakeyama (either side of the orange dashed line in Figures 7a and 7b): both AR and TR were high to the west, but low to the east. This difference was apparently caused by differences in the seismic velocity structure, as described below.

Figure 5. Forecast results for the Japan Meteorological Agency catalog off Iwate and Miyagi prefectures. (a) Alarm rates (gray shading), and the epicentral distribution of target earthquakes preceded by (solid blue circles) and not preceded by (open circles) foreshocks. The pink dashed rectangle indicates the Offshore Sanriku area of Uchida et al. (2016), and the orange dashed rectangle indicates the area of slow slip events estimated by Ito et al. (2013). The evaluation region is divided into regions N and S at 39°N. (b) Truth rates (gray shading), and the epicentral distribution of alarm earthquakes followed by (solid red circles) and not followed by (x-marks) a target earthquake. Note that the alarmed target earthquakes and alarm earthquakes were identified in each $D \times D$ on the center of grids arranged at $D/2$ intervals shown in Figure S1a. On the other hand, the grayed areas in (a), (b) are for an overview of the high and low areas of AR and TR without spatial duplication. (c) Time-space plot of the target earthquakes shown in (a). Pink stripes indicate the positive phases of the 3.09-year period obtained by the best-fitted sinusoidal function to data after 1984.5 estimated by Uchida et al. (2016), and gray stripes indicate retrospective positive phases. Vertical orange lines indicate the slow slip events period estimated by Ito et al. (2013). Green curves indicate the averaged cumulative slip of repeating earthquakes in regions N and S. (d) Time-space plot of the foreshock candidates shown in (b). Other details are the same as in (c).

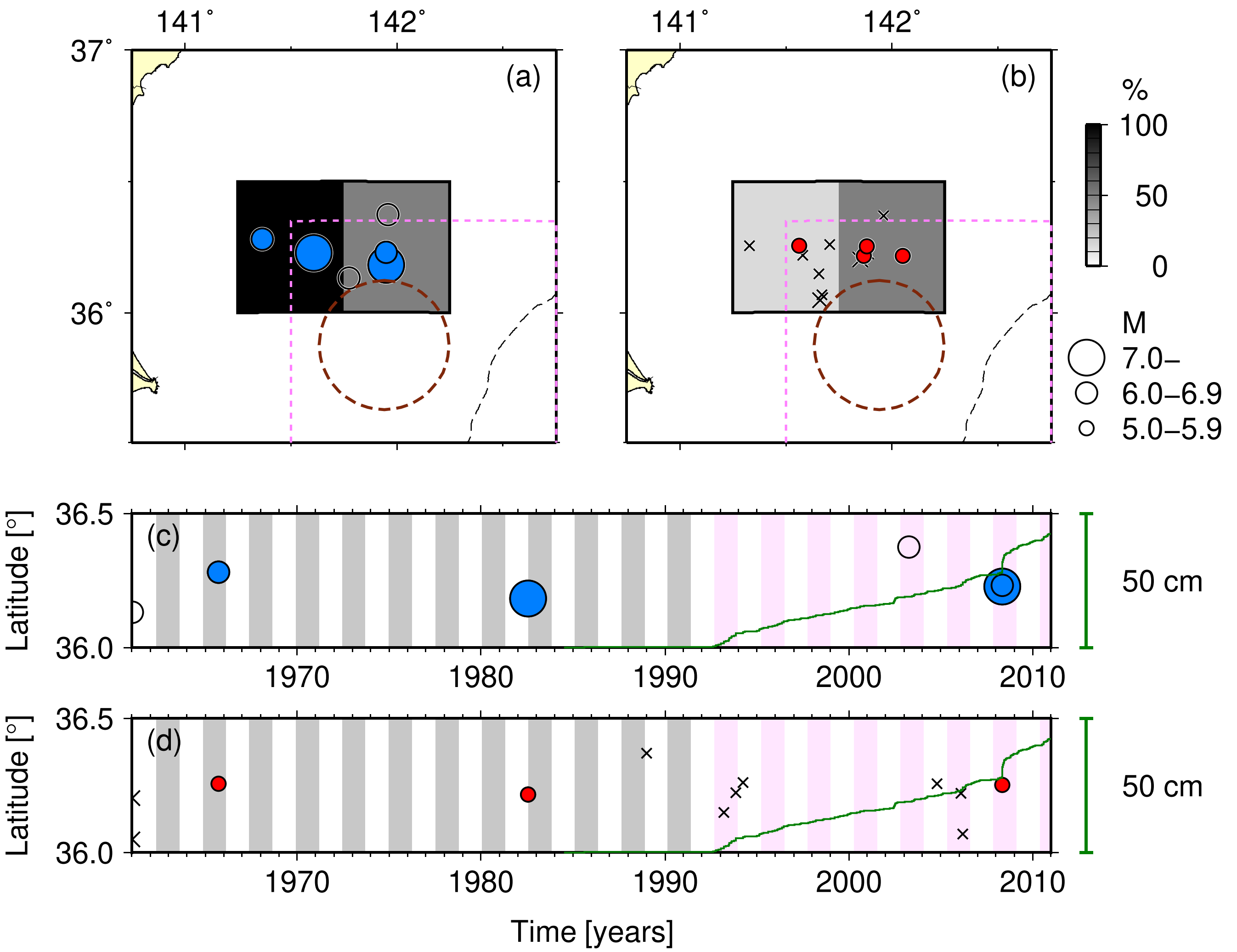

Figure 6. Same as Figure 5, but for off Ibaraki prefecture. (a), (b) The pink dashed rectangle indicates area H in Uchida et al. (2016). The brown dashed circle indicates a subducted seamount (Mochizuki et al., 2008). (c), (d) Pink stripes indicate the positive phases of the 2.53-year period obtained by the best-fitted sinusoidal function to data after 1992 estimated by Uchida et al. (2016), and gray stripes indicate retrospective positive phases. Green curves indicate the averaged cumulative slip of repeating earthquakes in the evaluation region.

Nakajima and Hasegawa (2007) showed by a 3D tomography study that the depth range of low-velocity anomalies changes along the NKTZ. West of Mt. Niigata-Yakeyama, a prominent low-velocity anomaly area extends from the upper crust to the uppermost mantle. Nakajima and Hasegawa (2007) suggested that the low-velocity anomaly might be caused by the presence of melts and a higher temperature zone resulting from the magmatic activity. Thus, swarms associated with fluid movement detected by Maeda's method might appear to be precursors (foreshocks) of target earthquakes. In contrast, east of Mt. Niigata-Yakeyama, a high-velocity anomaly area was observed in the crust. Thus, the situation in the NKTZ contrasts with that along the Japan trench, where no foreshocks occurred in low-velocity anomaly areas (cf., Section 5.1).

5.4. Izu Islands

In the Izu Islands, we adopted $D = 0.2°$ because it yielded the maximum ΔAIC among the three tested values (Table S2). Among 65 target earthquakes, 47 were alarmed (AR 72.3%); thus, AR was higher than in the other areas (Table 2, Figure 8). Among 314 alarm earthquakes, 63 were true foreshocks (TR 20.1%). Alarmed target earthquakes were distributed almost evenly along the Shichito-Ioto ridge (a line of active volcanoes) and the Zenisu ridge (Figure 1). Many alarmed target earthquakes occurred to the east of the

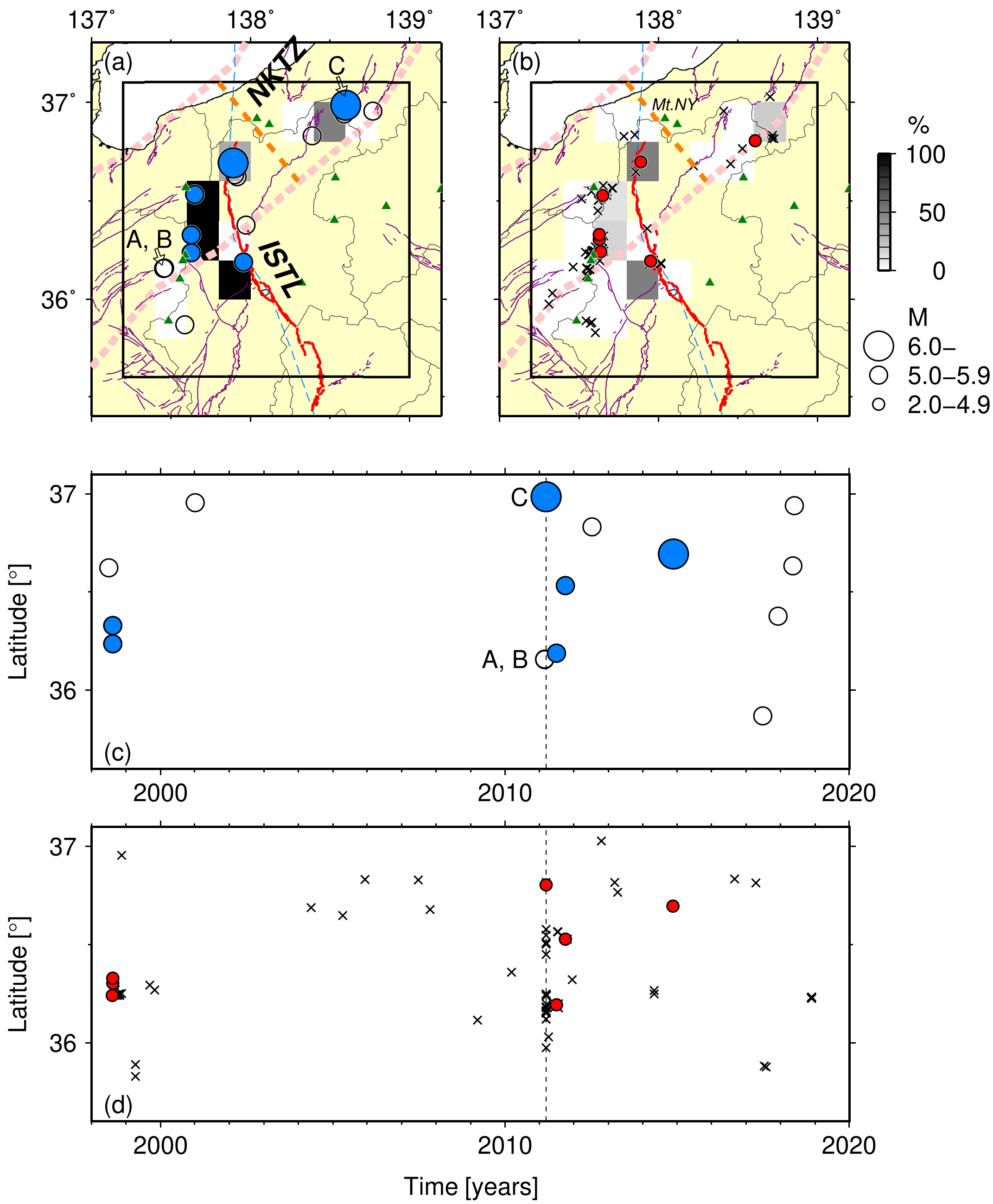

Figure 7. Same as Figure 5, but for central Honshu. (a), (b) The red line in (a), (b) indicates the Itoigawa-Shizuoka Tectonic Line (ISTL) (Headquarters for Earthquake Research Promotion, 2015a). The blue dashed line indicates the boundary between the Amur and Okhotsk plates at the Earth's surface (Bird, 2003). The Niigata-Kobe Tectonic Zone lies between the pink dashed lines (Sagiya et al., 2000). The orange dashed line indicates a velocity perturbation boundary in the crust (Nakajima & Hasegawa, 2007). Triangles indicate active volcanoes. Mt. NY indicates Mt. Niigata-Yakeyama. (c), (d) The vertical dashed line indicates the origin time (14:46 JST on March 11, 2011) of the M_w 9.0 Tohoku-oki earthquake. Event A, M 5.0 (2:18 JST on February 27, 2011); Event B, M 5.5 (5:38 JST on February 27, 2011); and Event C, M 6.7 (3:59 JST on March 12, 2011).

Izu Peninsula (around 35°N), and AR was high (e.g., 92.3% = 12/13%, and 83.3% = 5/6). In the eastern Izu region, swarm rate changes coincided with changes in volumetric strain increments caused by magma intrusions (e.g., Kumazawa et al., 2016). Maeda's method tends to detect swarms associated with magmatic activity as precursors (foreshocks) of target earthquakes.

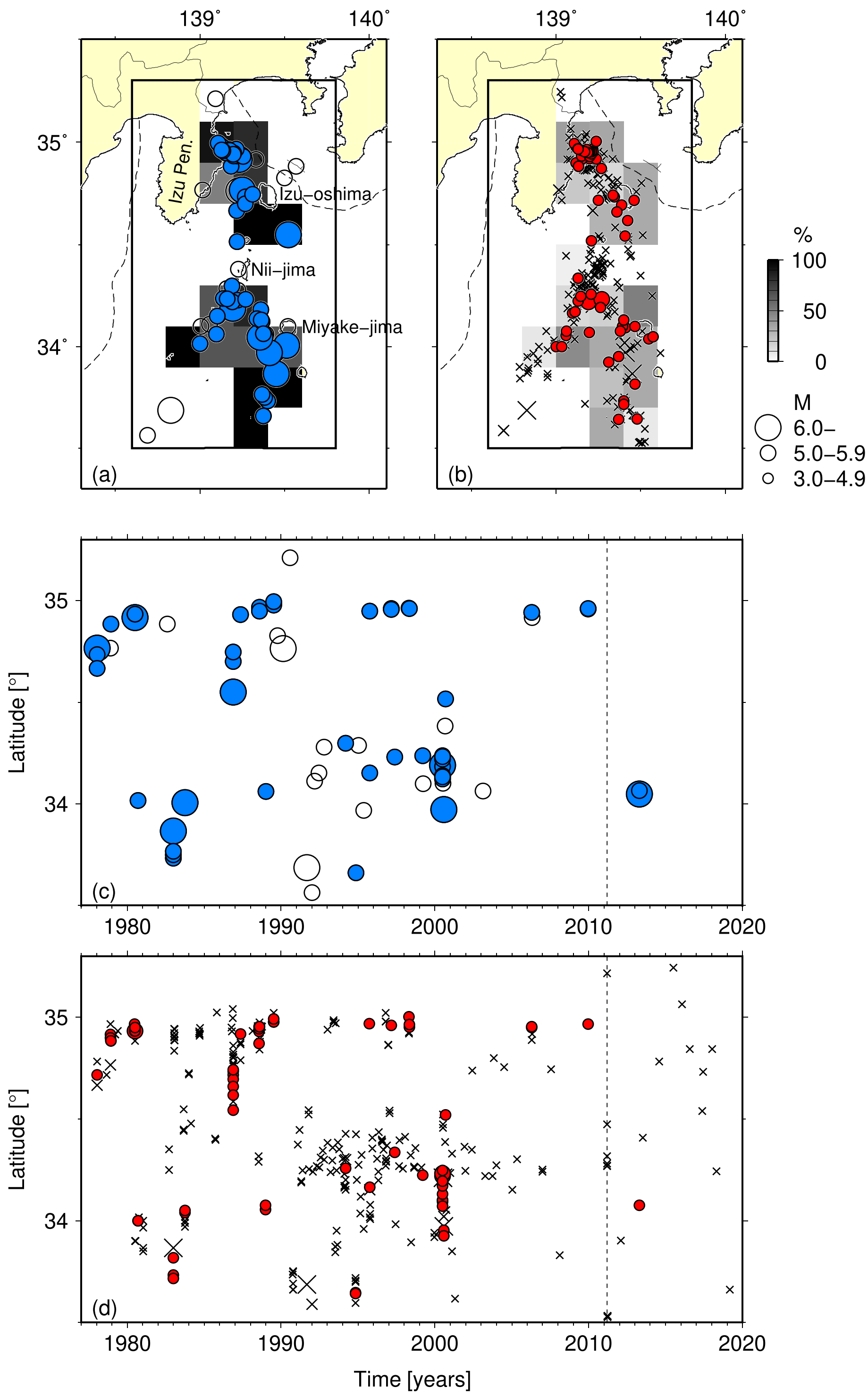

Figure 8. Same as Figure 5, but for the Izu Islands. (c, d) The vertical dashed line indicates the origin time of the M_w 9.0 mainshock.

Around Nii-jima island (34.3–34.5°N, 139.2–139.4°E), 27 false alarm earthquakes occurred frequently, especially during 1990–2000. During this period, although the seismicity rate and maximum event magnitude tended to increase from year to year, a target earthquake did not occur. A structural investigation along the Shichito-Ioto ridge showed that the middle crust is thinner beneath Nii-jima island than beneath

Izu-oshima and Miyake-jima islands (Kodaira et al., 2007). Nii-jima island is a rhyolitic volcano whereas Izu-oshima and Miyake-jima are basaltic volcanoes. Differences in the lithologic character and growth process of the middle crust may thus affect the occurrence of target earthquakes near these islands. More study is needed to clarify the relation between these features and foreshock activity. Note that the seismicity rate decreased overall after 2000 (see Section s1 and Figure S5), and the number of target earthquakes also decreased (Figure 8c). Although the number of alarm earthquakes increased just after the M_w 9 event, they were not followed by target earthquakes. Therefore, the earthquakes induced by the M_w 9 event may have ruptured only small asperity patches without the occurrence of a cascade-up process (Noda et al., 2013) owing to the high strength of a large patch.

5.5. Suggestions for Future Work

We used all earthquakes along the Japan trench shallower than 100 km because the depth precision of offshore earthquakes is insufficient. However, interplate and intraplate earthquakes occur together in double seismic planes in the Pacific slab (Gamage et al., 2009). As the ocean-bottom seismometer network becomes denser, it may be possible to improve forecast efficiency by selecting earthquakes based on fault parameters.

The finding that foreshocks off Iwate and Miyagi prefectures are excited by periodic SSEs is very useful information. However, because increased aftershock and afterslip activities since the M_w 9 event have overshadowed periodic SSEs, continuous monitoring will be necessary to detect the possible reactivation of periodic SSEs.

Because Maeda's method is a forecast model based on short-term foreshocks, the lead time from an alarm earthquake to a target earthquake is only several days. A comprehensive forecast model (Aki, 1981) that takes into consideration mid-to-long term precursors such as changes of the *b* value in the Gutenberg-Richter law (Nanjo et al., 2012), tidal correlation (Tanaka, 2012), and seismic quiescence (Katsumata, 2011) is needed. In addition, by taking into consideration differences in magnitude, time, and epicentral distance between the mainshock and largest foreshock (Tamaribuchi et al., 2018), we may be able to constrain the alarmed area and magnitude.

6. Conclusions

We investigated the effectiveness of earthquake forecast by Maeda's method that extracted precursory swarm activity under various tectonic environments of Japan such as regions characterized by interplate seismic activity, a tectonic fault line (concentrated deformation zone), and an island arc area of seismic and volcanic activity. We compared Maeda's method with not only random guesses but also the ETAS forecast based on the stationary space-time ETAS model. As a result, we confirmed the forecast efficiency of Maeda's method was generally higher (Section 4.1). Besides, the synthetic ETAS catalog analysis showed that the seismicity immediately before target earthquakes was more active in the real catalog, and the comprehensive forecast efficiency index F-measure was higher when Maeda's method is applied to the real catalog than to the synthetic ETAS catalogs (Section 4.2). To summarize, Maeda's method is a simple and efficient counting-number-based earthquake forecast model and may capture characteristics of foreshocks that reflect a physical phenomenon, such as a nucleation process involving precursory slip, which the stationary ETAS model is not able to represent.

We also found that foreshocks along the Japan trench were distributed along the edges of low-velocity anomaly areas and among areas of background swarms that correspond to SSEs (Section 5). Those foreshocks may be caused by a heterogeneous stress distribution associated with the existence of a plate-bending axis and a subducted seamount. In particular, foreshocks off Iwate and Miyagi prefectures were excited by periodic SSEs. In the inland tectonic zone and the island arc, swarm activity associated with magmatic or fluid activity tended to precede a target earthquake.

Data Availability Statement

Plate boundary data at the Earth's surface were taken from Bird (2003; https://agupubs.onlinelibrary.wiley.com/doi/full/10.1029/2001GC000252). Plate convergence rate data were calculated using the Plate Motion Calculator at the UNAVCO website (https://www.unavco.org/).

Acknowledgments

We thank all of the contributing institutions and universities and the JMA for providing the unified hypocenter catalog. We used the R software package "ETAS" (Jalilian, 2019; https://github.com/jalilian/ETAS) to estimate the parameters of the stationary space-time ETAS model. We also used catalogs of low-frequency tremors, very low frequency earthquakes, and background swarms (Nishikawa et al., 2019, https://sites.google.com/site/tomoakinishikawahomepage/). We thank Dr. Zhao Depeng and Katayama Yu for providing data of seismic velocity perturbations on the upper boundary of the subducting Pacific slab. We used the catalog of small repeating earthquakes (Table S1 of Uchida et al., 2016) and digital bathymetric data provided by the Hydrographic and Oceanographic Department of the Japan Coast Guard, Japan Oceanographic Data Center (https://jdoss1.jodc.go.jp/vpage/depth500_file_j.html). Figures were prepared by using GMT (Wessel et al., 2013). This manuscript was greatly improved by careful reviews of two anonymous reviewers. This study was supported by the Ministry of Education, Culture, Sports, Science and Technology (MEXT) of Japan, under its The Second Earthquake and Volcano Hazards Observation and Research Program (Earthquake and Volcano Hazard Reduction Research).

References

Aki, K. (1981). A probabilistic synthesis of precursory phenomena. In D. W. Simpson, & P. G. Richards (Eds.), A probabilistic synthesis of precursory phenomena, Earthquake Prediction (Vol.4, pp. 566–574). Maurice Ewing Series. AGU. https://doi.org/10.1029/ME004p0566

Bird, P. (2003). An updated digital model of plate boundaries. *Geochemistry, Geophysics, Geosystems*, *4*(3), 1027. https://doi.org/10.1029/2001GC000252

Bouchon, M., Durand, V., Marsan, D., Karabulut, H., & Schmittbuhl, J. (2013). The long precursory phase of most large interplate earthquakes. *Nature Geoscience*, *6*, 299–302. https://doi.org/10.1038/NGEO1770

Bouchon, M., & Marsan, D. (2015). Reply to 'Artificial seismic acceleration'. *Nature Geoscience*, *8*, 83–83. https://doi.org/10.1038/ngeo2359

Console, R., Murru, M., & Falcone, G. (2010). Probability gains of an epidemic-type aftershock sequence model in retrospective forecasting of $M \geq 5$ earthquakes in Italy. *Journal of Seismology*, *14*, 9–26. https://doi.org/10.1007/s10950-009-9161-3

DeMets, C., Gordon, R. G., & Argus, D. F. (2010). Geologically current plate motions. *Geophysical Journal International*, *181*, 1–80. https://doi.org/10.1111/j.1365-246X.2009.04491.x

Felzer, K. R., Abercrombie, R. E., & Ekström, G. (2004). A common origin for aftershocks, foreshocks, and multiplets. *Bulletin of the Seismological Society of America*, *94*, 88–98. https://doi.org/10.1785/0120030069

Felzer, K. R., Page, M. T., & Michael, A. J. (2015). Artificial seismic acceleration. *Nature Geoscience*, *8*, 82–83. https://doi.org/10.1038/ngeo2358

Fujie, G., Ito, A., Kodaira, S., Takahashi, N., & Kaneda, Y. (2006). Confirming sharp bending of the Pacific plate in the northern Japan trench subduction zone by applying a traveltime mapping method. *Physics of the Earth and Planetary Interiors*, *157*, 72–85. https://doi.org/10.1016/j.pepi.2006.03.013

Gamage, S. S. N., Umino, N., Hasegawa, A., & Kirby, S. H. (2009). Offshore double-planed shallow seismic zone in the NE Japan forearc region revealed by sP depth phases recorded by regional networks. *Geophysical Journal International*, *178*, 195–214. https://doi.org/10.1111/j.1365-246X.2009.04048.x

Headquarters for Earthquake Research Promotion. (2015a). *Long-term evaluation of Itoigawa-Shizuoka tectonic line fault zone* (2nd ed., p. 60). (in Japanese). Retrieved from https://www.jishin.go.jp/main/chousa/katsudansou_pdf/41_42_44_itoigawa-shizuoka_2.pdf

Hirose, F., Miyaoka, K., Hayashimoto, N., Yamazaki, T., & Nakamura, M. (2011). Outline of the 2011 off the Pacific Coast of Tohoku Earthquake (Mw9.0)- Seismicity: Foreshocks, mainshock, aftershocks, and induced activity -. *Earth Planets and Space*, *63*, 513–518. https://doi.org/10.5047/eps.2011.05.019

Hua, Y., Zhao, D., Toyokuni, G., & Xu, Y. (2020). Tomography of the source zone of the great 2011 Tohoku earthquake. *Nature Communications*, *11*, 1163. https://doi.org/10.1038/s41467-020-14745-8

Ito, Y., Hino, R., Kido, M., Fujimoto, H., Osada, Y., Inazu, D., et al. (2013). Episodic slow slip events in the Japan subduction zone before the 2011 Tohoku-Oki earthquake. *Tectonophysics*, *600*, 14–26. https://doi.org/10.1016/j.tecto.2012.08.022

Jalilian, A. (2019). ETAS: An R package for fitting the space-time ETAS model to earthquake data. *Journal of Statistical Software*, *88*, Code Snippet 1. https://doi.org/10.18637/jss.v088.c01

Katsumata, K. (2011). A long-term seismic quiescence started 23 years before the 2011 off the Pacific coast of Tohoku Earthquake (M = 9.0). *Earth Planets and Space*, *63*, 709–712. https://doi.org/10.5047/eps.2011.06.033

Kodaira, S., Sato, T., Takahashi, N., Ito, A., Tamura, Y., Tatsumi, Y., & Kaneda, Y. (2007). Seismological evidence for variable growth of crust along the Izu intraoceanic arc. *Journal of Geophysical Research: Solid Earth*, *112*, B05104. https://doi.org/10.1029/2006JB004593

Kumazawa, T., & Ogata, Y. (2014). Nonstationary ETAS models for nonstandard earthquakes. *Annals of Applied Statistics*, *8*, 1825–1852. https://doi.org/10.1214/14-AOAS759

Kumazawa, T., Ogata, Y., Kimura, K., Maeda, K., & Kobayashi, A. (2016). Background rates of swarm earthquakes that are synchronized with volumetric strain changes. *Earth and Planetary Science Letters*, *442*, 51–60. https://doi.org/10.1016/j.epsl.2016.02.049

Lippiello, E., Godano, C., & de Arcangelis, L. (2019). The relevance of foreshocks in earthquake triggering: A statistical study. *Entropy*, *21*, 173. https://doi.org/10.3390/e21020173

Lippiello, E., Marzocchi, W., de Arcangelis, L., & Godano, C. (2012). Spatial organization of foreshocks as a tool to forecast large earthquakes. *Scientific Reports*, *2*, 846. https://doi.org/10.1038/srep00846

Llenos, A. L., McGuire, J. J., & Ogata, Y. (2009). Modeling seismic swarms triggered by aseismic transients. *Earth and Planetary Science Letters*, *281*, 59–69. https://doi.org/10.1016/j.epsl.2009.02.011

Llenos, A. L., & Michael, A. J. (2019). Ensembles of ETAS models provide optimal operational earthquake forecasting during swarms: Insights from the 2015 San Ramon, California swarm. *Bulletin of the Seismological Society of America*, *109*, 2145–2158. https://doi.org/10.1785/0120190020

Maeda, K. (1993). An empirical alarm criterion based on immediate foreshocks: A case study for the Izu region (in Japanese with English abstract). *Journal of the Seismological Society of Japan*, *45*, 373–383. https://doi.org/10.4294/zisin1948.45.4_373

Maeda, K. (1996). The use of foreshocks in probabilistic prediction along the Japan and Kuril trenches. *Bulletin of the Seismological Society of America*, *86*, 242–254.

Maeda, K., & Hirose, F. (2016). Empirical forecast of occurrence of mainshocks based on foreshock activities (in Japanese with English figure caption). *Report of the Coordinating Committee for Earthquake Prediction*, *95*, 415–419.

Mochizuki, K., Yamada, T., Shinohara, M., Yamanaka, Y., & Kanazawa, T. (2008). Weak interplate coupling by seamounts and repeating M ~ 7 earthquakes. *Science*, *321*, 1194–1197. https://doi.org/10.1126/science.1160250

Molchan, G. M. (1997). Earthquake prediction as a decision-making problem. *Pure and Applied Geophysics*, *149*, 233–247. https://doi.org/10.1007/BF00945169

Nakajima, J., & Hasegawa, A. (2007). Deep crustal structure along the Niigata-Kobe Tectonic Zone, Japan: Its origin and segmentation. *Earth Planets and Space*, *59*, e5–e8. https://doi.org/10.1186/BF03352677

Nakatani, M. (2020). Evaluation of phenomena preceding earthquakes and earthquake predictability. *Journal of Disaster Research*, *15*, 112–143. https://doi.org/10.20965/jdr.2020.p0112

Nanjo, K. Z., Hirata, N., Obara, K., & Kasahara, K. (2012). Decade-scale decrease in b value prior to the M9-class 2011 Tohoku and 2004 Sumatra quakes. *Geophysical Research Letters*, *39*, L20304. https://doi.org/10.1029/2012GL052997

Nishikawa, T., Matsuzawa, T., Ohta, K., Uchida, N., Nishimura, T., & Ide, S. (2019). The slow earthquake spectrum in the Japan Trench illuminated by the S-net Seafloor observatories. *Science*, *365*, 803–813. https://doi.org/10.1126/science.aax5618

Noda, H., Nakatani, M., & Hori, T. (2013). Large nucleation before large earthquakes is sometimes skipped due to cascade-up—Implications from a rate and state simulation of faults with hierarchical asperities. *Journal of Geophysical Research: Solid Earth*, *118*, 2924–2952. https://doi.org/10.1002/jgrb.50211

Ogata, Y. (1988). Statistical models for earthquake occurrences and residual analysis for point processes. *Journal of the American Statistical Association*, *83*, 9–27. https://doi.org/10.1080/01621459.1988.10478560

Ogata, Y., & Katsura, K. (2014). Comparing foreshock characteristics and foreshock forecasting in observed and simulated earthquake catalogs. *Journal of Geophysical Research: Solid Earth*, *119*, 8457–8477. https://doi.org/10.1002/2014JB011250

Ogata, Y., & Zhuang, J. (2006). Space-time ETAS models and an improved extension. *Tectonophysics*, *413*(1–2), 13–23. https://doi.org/10.1016/j.tecto.2005.10.016

Petrillo, G., & Lippiello, E. (2021). Testing of the foreshock hypothesis within an epidemic like description of seismicity. *Geophysical Journal International*, *225*, 1236–1257. https://doi.org/10.1093/gji/ggaa611

Sagiya, T., Miyazaki, S., & Tada, T. (2000). Continuous GPS array and present-day crustal deformation of Japan. *Pure and Applied Geophysics*, *157*, 2303–2322. https://doi.org/10.1007/PL00022507

Seif, S., Zechar, J. D., Mignan, A., Nandan, S., & Wiemer, S. (2019). Foreshocks and their potential deviation from general seismicity. *Bulletin of the Seismological Society of America*, *109*, 1–18. https://doi.org/10.1785/0120170188

Tamaribuchi, K. (2018). Evaluation of automatic hypocenter determination in the JMA unified catalog. *Earth Planets and Space*, *70*, 141. https://doi.org/10.1186/s40623-018-0915-4

Tamaribuchi, K., Yagi, Y., Enescu, B., & Hirano, S. (2018). Characteristics of foreshock activity inferred from the JMA earthquake catalog. *Earth Planets and Space*, *70*, 90. https://doi.org/10.1186/s40623-018-0866-9

Tanaka, S. (2012). Tidal triggering of earthquakes prior to the 2011 Tohoku-Oki earthquake (Mw 9.1). *Geophysical Research Letters*, *39*, L00G26–n. https://doi.org/10.1029/2012GL051179

Tsuru, T., Park, J., Miura, S., Kodaira, S., Kido, Y., & Hayashi, T. (2002). Along-arc structural variation of the plate boundary at the Japan Trench margin: Implication of interpolate coupling. *Journal of Geophysical Research: Solid Earth*, *107*, 2357–2361. https://doi.org/10.1029/2001JB001664

Uchida, N., Iinuma, T., Nadeau, R. M., Bürgmann, R., & Hino, R. (2016). Periodic slow slip triggers megathrust zone earthquakes in northeastern Japan. *Science*, *351*(6272), 488–492. https://doi.org/10.1126/science.aad3108

Utsu, T. (1961). A statistical study on the occurrence of aftershocks. *Geophysical Magazine*, *30*, 521–605.

Utsu, T. (1970). Aftershocks and earthquake statistics (II)- Further investigation of aftershocks and other earthquake sequences based on a new classification of earthquake sequences-. *Journal of the Faculty of Science, Hokkaido University - Series 7: Geophysics*, *3*(4), 197–266.

Utsu, T. (1999). Representation and analysis of the earthquake size distribution: A historical review and some new approaches. *Pure and Applied Geophysics*, *155*(2–4), 509–535. https://doi.org/10.1007/s000240050276

Wessel, P., Smith, W. H. F., Scharroo, R., Luis, J., & Wobbe, F. (2013). Generic mapping tools: Improved version released. *Eos, Transactions American Geophysical Union*, *94*(45), 409–410. https://doi.org/10.1002/2013EO450001

Zhuang, J., Ogata, Y., & Wang, T. (2017). Data completeness of the Kumamoto earthquake sequence in the JMA catalog and its influence on the estimation of the ETAS parameters. *Earth Planets and Space*, *69*, 36. https://doi.org/10.1186/s40623-017-0614-6

References From the Supporting Information

Gutenberg, B., & Richter, C. F. (1944). Frequency of earthquakes in California. *Bulletin of the Seismological Society of America*, *34*, 185–188. https://doi.org/10.1785/bssa0340040185

Headquarters for Earthquake Research Promotion. (2015b). *Long-term evaluation of faults along the western margin of the Nagano basin*. (revision) (in Japanese) (pp. 34). Retrieved from https://www.jishin.go.jp/main/chousa/katsudansou_pdf/40_shinanogawa_2.pdf

Japan Meteorological Agency. (2006). *Report on the eruption of Miyakejima volcano and seismic activity around Niijima and Kozushima in 2000*. Technical report of the Japan Meteorological Agency (in Japanese with English abstract).

Ogata, Y. (1981). On Lewis' simulation method for point processes. *IEEE Transactions on Information Theory*, *IT-27*, 23–31. https://doi.org/10.1109/TIT.1981.1056305

Ogata, Y. (1998). Space-time point-process models for earthquake occurrences. *Annals of the Institute of Statistical Mathematics*, *50*, 379–402. https://doi.org/10.1023/A:1003403601725

Okino, K., Shimakawa, Y., & Nagaoka, S. (1994). Evolution of the Shikoku Basin. *Journal of Geomagnetism and Geoelectricity*, *46*(6), 463–479. https://doi.org/10.5636/jgg.46.463

Ross, G. J. (2021). Bayesian estimation of the ETAS model for earthquake occurrences. *Bulletin of the Seismological Society of America*, *111*, 1473–1480. https://doi.org/10.1785/0120200198

Schoenberg, F. P., Chu, A., & Veen, A. (2010). On the relationship between lower magnitude thresholds and bias in epidemic-type aftershock sequence parameter estimates. *Journal of Geophysical Research: Solid Earth*, *115*, B04309. https://doi.org/10.1029/2009JB006387

Seno, T., & Maruyama, S. (1984). Paleogeographic reconstruction and origin of the Philippine Sea. *Tectonophysics*, *102*(1–4), 53–84. https://doi.org/10.1016/0040-1951(84)90008-8

Takahashi, M. (1994). Miocene lateral bending of central Japan- Intra-arc deformation at arc-arc collision zone -. *Bulletin of the Geological Survey of Japan*, *45*(8/9), 477–495.

Zhuang, J., Ogata, Y., & Vere-Jones, D. (2002). Stochastic declustering of space-time earthquake occurrences. *Journal of the American Statistical Association*, *97*, 369–380. https://doi.org/10.1198/016214502760046925